Tests of Scintillator+WLS strips for Muon System at Future Colliders

Dmitri Denisov*, Valery Evdokimov‡, Strahinja Lukić [1)]†

† *Vinča Institute, University of Belgrade, Serbia*
‡ *Institute for High Energy Physics, Protvino, Russia*
* *Fermilab, Batavia IL, USA*

Abstract

Prototype scintilator+WLS strips with SiPM readout for muon system at future colliders were tested for light yield, time resolution and position resolution. Depending on the configuration, light yield of up to 36 photoelectrons per muon per SiPM has been achieved, as well as time resolution of 0.5 ns and position resolution of ~ 7 cm.

[1] slukic@vinca.rs

Operated by Fermi Research Alliance, LLC under Contract No. De-AC02-07CH11359 with the United States Department of Energy.

1 Introduction

Several concepts of future colliders, including e^+e^- colliders, are currently under study for the next generation of particle experiments [1–3]. Due to the well-defined initial state of the interactions, low backgrounds and radiation levels, e^+e^- colliders are an attractive option for precision measurements to test various theoretical extensions of the Standard Model in the areas where the predictions of the competing models differ by a few percent, such as, e.g. in the Higgs sector.

The detector concepts for the future e^+e^- colliders have been developed to a high level of detail over the past decade. Since the publication of the LoI of the two major concepts, the SiD [4] and the ILD [5], numerous technical details have been specified to an advanced level. R&D prototypes of inividual subsystems reach levels of complexity involving hundreds of thousands of readout channels (See e.g. Ref. [6]).

However, for the muon systems relatively few specific details are defined. A promising option for the muon system consists of scintillator strips with WLS fibers and SiPM readout built into the magnet yoke of a detector in several layers [7]. In such a system, the coordinates of the muon track are reconstructed using the observables such as the coordinate of the strip hit by a passing muon and the signal time difference between the ends of the strip to measure position along the strip.

The present study is the first in a series devoted to the study of the time resolution and the position resolution achievable from the time difference between the ends of scintillator strips with WLS fibers and SiPM readout. The measurements described in this paper have been performed using cosmic muons at the location of the DØ assembly building at the Fermi National Accelerator Laboratory, Batavia, USA, at the elevation of 220 m above sea level. The local cosmic muon fluence has been measured previously by the MicroBooNE collaboration to be $\sim 100\ \mathrm{m}^{-2}\ \mathrm{s}^{-1}$, with a peak energy between 1 and 2 GeV [8].

Hamamatsu S10931-050P SiPM were used for the test [9].

Section 2 describes the measurement setups that were used, Sec. 3 describes time- and amplitude calibration procedures, Sec. 4 describes the tested scintillator strip – WLS fiber configurations, Sec. 5 gives details on the data analysis procedures, Sec. 6 tabulates the measurement results. Conclusions are given in Sec. 7.

2 Measurement Setup

Two setups that were used for the measurements are described here. In both setups cosmic muons are detected by coincidence between three vertically arranged scintillation counters.

A CAMAC system with a LeCroy 2249A 12-input charge-sensitive ADC and a LeCroy 2228A 8-input TDC was used to digitize the amplitude and the arrival time of the signals. The data collection was performed and monitored from a PC with USB connection to the CAMAC Crate controller of type CC-USB by Wiener Plein&Baus, using custom-made software [10].

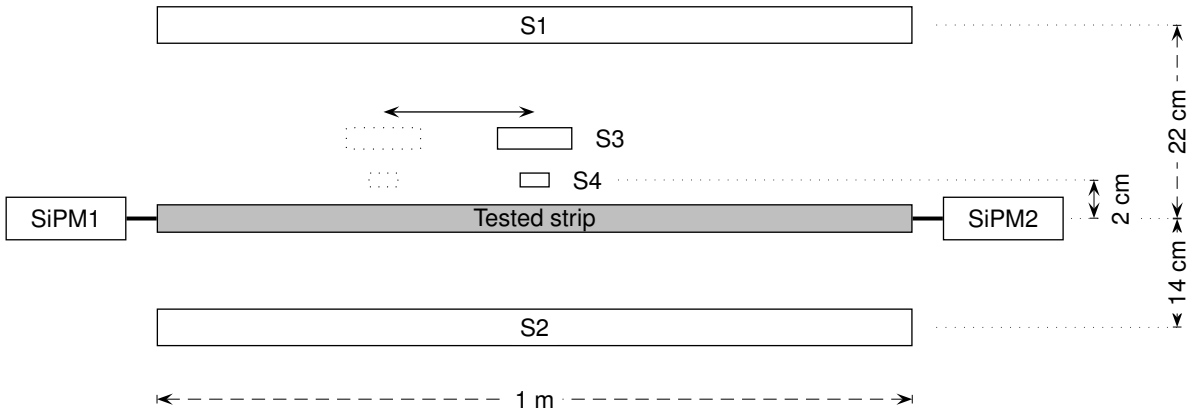

Figure 1: Schematic of the test setup with scintillator pads restricting cosmic muon position by coincidence. S1 and S2 are scintillation counters with vacuum PMT positioned above and below the tested strip. S3 and S4 are small-area scintillators with vacuum PMT used to select events where the muon hits a given location along the tested strip. The location of S3 and S4 w.r.t the tested strip was changed from run to run, keeping the relative position of S3 and S4 always the same. SiPM1 and SiPM2 represent the SiPM connected to the respective ends of the WLS fiber of the tested strip.

2.1 Setup 1

Setup 1 is shown in Fig. 1. S1 and S2 are plastic scintillation counters with vacuum PMT located above and below the tested strip, each of them 1 m long, 10 cm wide and 1 cm thick, used to detect the passage of a muon by coincidence requirement. S3 and S4 are scintillation counters with vacuum PMT used to restrict the location of the muon along the tested strip by coincidence requirement. S3 is a 10×15 cm plastic scintillator pad oriented with its 10 cm side along the tested strip. S4 is a 40 cm long and 2.7 cm wide Bicron© 404A strip oriented across the tested strip. The distance from the center of the tested strip to the PMT of S4 was 5 cm.

The location of S3 and S4 along the tested strip was changed from run to run in order to study different points along the tested strip, keeping the relative position of S3 and S4 always the same. SiPM1 and SiPM2 denote the SiPM connected to the respective ends of the WLS fiber of the tested strip. The vertical distance between S1 and the tested prototype is 22 cm, and the vertical distance between S2 and the tested prototype is 14 cm. The distance of S4 to the tested prototype was 2 cm. The length of the tested strips was 1 m.

Coincidence between S1, S2 and S3 was used as the trigger, signalling the passage of a muon. The signal from S3 was delayed by 20 ns with respect to the signals from S1 and S2, so that the trigger signal is always formed at the rising edge of the S3 signal. In the offline analysis, the presence of the signal in S4 was required for event selection.

When measuring properties close to either end of the tested strip, the counters S1 and S2 were moved along the axis in order to cover locations up to at least 20 cm beyond the end of the tested strip. This was done in order to prevent loss of the muon flux, which would have caused a loss of

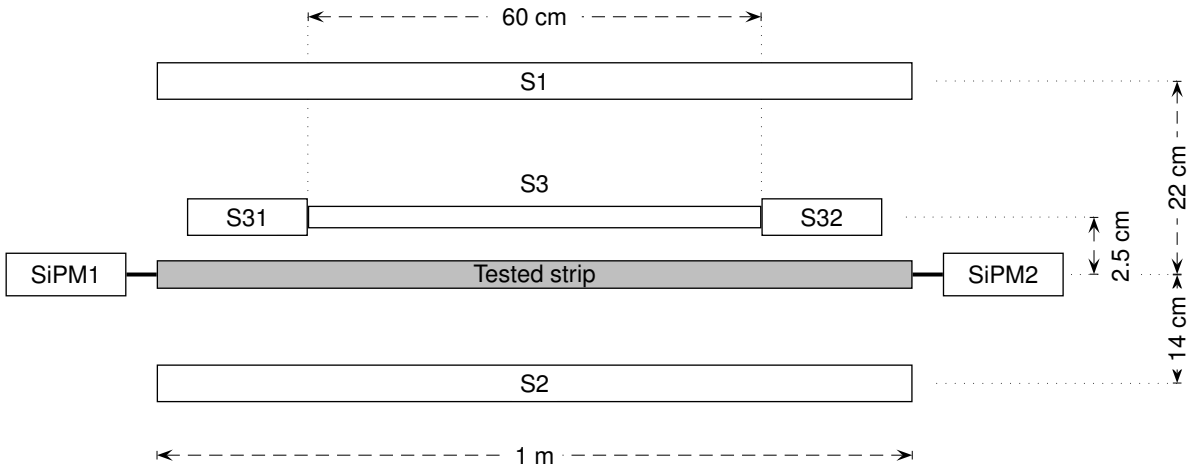

Figure 2: Schematic of the test setup with a scintillator strip with fast PMT for the muon position determination. S1 and S2 are scintillation counters with vacuum PMT positioned above and under the tested strip. S31 and S32 are vacuum PMTs attached to both ends of a scintillator strip located at a 2.5 cm distance vertically from the tested strip. SiPM1 and SiPM2 represent the SiPMs connected to the respective ends of the WLS fiber of the tested strip.

statistic and a muon position bias at these points.

The signals from the counters S1 and S2 were used only for triggering. The signals from S3, S4, SiPM1 and SiPM2 were recorded. Each of the signals to be recorded was first split into the time- and the amplitude channels using linear fan-in fan-out modules. The time signals were processed using constant threshold discriminators. The time signals were delayed by ~ 50 ns and digitized by the TDC CAMAC module using the trigger signal as the start. The amplitude signals were delayed by $\sim 30-40$ ns and digitized by the ADC CAMAC module, using gate generated by the trigger signal.

2.2 Setup 2

In setup 2 (Fig. 2) a Bicron© 404A scintillator strip, S3, was used to determine the location of the muon impact using the time difference between both ends readout by vacuum PMTs, S31 and S32. The length of S3 is 60 cm, the width 2.7 cm and the thickness 1.2 cm. The counters S1 and S2 are the same as in setup 1, located in the same way as in setup 1.

Coincidence between S1, S2 and S31 was used as the trigger, signalling the passage of a muon. The time signal of S31 was delayed by 20 ns with respect to the signals of S1 and S2, so that the trigger signal is formed at the rising edge of the S31 counter signal.

The signals from S1 and S2 were used only for triggering. The time and amplitude of the signals from S31, S32, SiPM1 and SiPM2 were digitized in the same way as in setup 1.

3 Calibration

3.1 ADC calibration and SiPM cross-talk factor

Calibration of the ADC response in terms of the number of photons detected by the SiPM was performed by illuminating SiPM with short LED pulses. The driving voltage for the LED had a triangular pulse shape. The amplitude of the driver signal necessary to provide light intensity at which on average 1 photon is detected was 1.1 V. Amplitudes up to 1.22 V were used to create spectra with up to 6 photons on average for the calibration. The width of the driver pulse at the 1 V level was ~ 2.5 ns. The stability of the amplitude was controlled by recording an inverted driver signal in a separate ADC channel.

Figure 3 shows an example of the measured ADC spectrum from a SiPM. The peaks in the spectrum correspond to integer numbers of pixels that fire. When the light intensty is low the *pedestal* peak, corresponding to the events in which no pixels have fired, is visible. The centroid of the pedestal peak and the average distance between the centroids of the neighboring peaks are used as calibration constants to express the signal amplitude in terms of the number of pixels that have fired, n_{pixel}.

Each detected photon may cause 1 or more pixels to fire. The ratio of the average number of fired pixels, $\langle n_{pixel} \rangle$, to the average number of detected photons, ν, is generally larger than 1 due to the optical and electrical cross-talks, as well as the afterpulsing (See eg. [11]). For simplicity we combine all these effects under the common *cross-talk factor* $X = \langle n_{pixel} \rangle / \nu$.

Considering the high number of pixels (3600) in the SiPMs used in the tests, the distribution of the number of detected photons at low light intensity is Poissonian to a very good approximation. Thus the probability for detecting zero photons is $P_0 = e^{-\nu}$. P_0 is measured as the ratio of the event number in the pedestal peak, A_0, to the integral of the whole spectrum, A, allowing to extract the average number of detected photons as $\nu = \ln(A_0/A)$. On the other hand, the average number of fired pixels is determined from the mean of the measured spectrum. Thus the cross-talk factor is obtained as,

$$X = -\frac{\langle n_{pixel} \rangle}{\ln(A_0/A)} \tag{1}$$

The cross-talk factor depends on several parameters, including the bias voltage applied to the SiPM and temperature. The bias voltage was kept constant to within 0.1 V for the duration of the tests. The experimental room was climatized, limiting the temperature variations. During the tests, the value of the cross-talk factor was measured several times, and the results were centered around $X = 1.35$ with relative variations up to $\pm 5\%$.

3.2 TDC calibration

The calibration of the TDC was performed using a setup schematically presented in Fig. 4. Pulses from a counter were brought to the input of one of the constant threshold discriminators. One of the

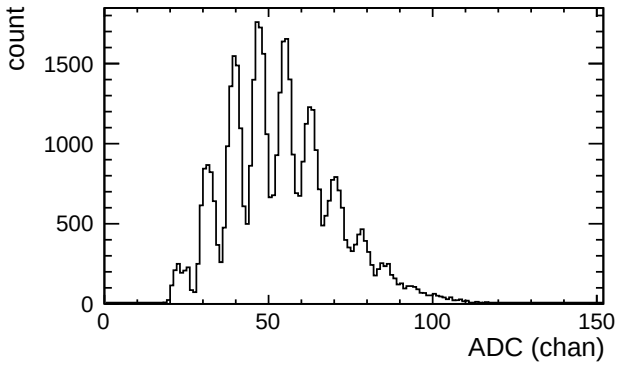

Figure 3: ADC spectrum of a SiPM illuminated by LED pulses.

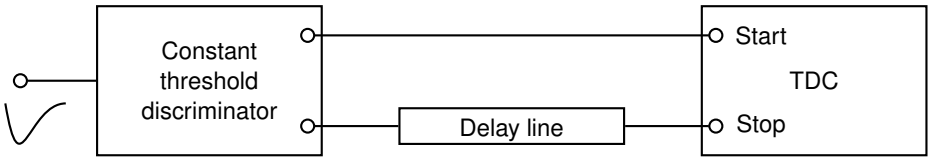

Figure 4: Schematic diagram of the circuit used for the TDC calibration.

logical outputs of the discriminator was used as the start signal for the TDC, while another, after passing through a delay line made of cables of known signal propagation time was used as the stop signal. Delays of 0, 3, 5, 8, 13 and 16 ns were used in addition to the constant difference in cable length between the start and the stop channels. Straight line was fitted to the graph of the delay times vs. the centroids of the recorded TDC spectra. The average calibration factor 0.1106 ns/bin was obtained from the slope of the fitted line for the 4 used TDC channels, with relative deviations up to 1% for the individual channels.

4 Tested configurations

Four configurations of the scintillator strip with WLS fibers were tested for the light yield. The description of the four configurations, denoted *A*, *B*, *C* and *D*, is given in the following subsections and schematically presented in Fig. 5. The configurations were designed based on the experience from the upgrade of the DØ muon system [12]. Two configurations with the best light yield were selected for detailed position- and time-resolution tests.

4.1 Configuration *A*

Configuration *A* consisted of a 1 m long clear polystyrene scintillator strip with a 41×10 mm^2 profile, co-extruded with a TiO_2 loaded polystyrene layer such as used by the MINOS collabora-

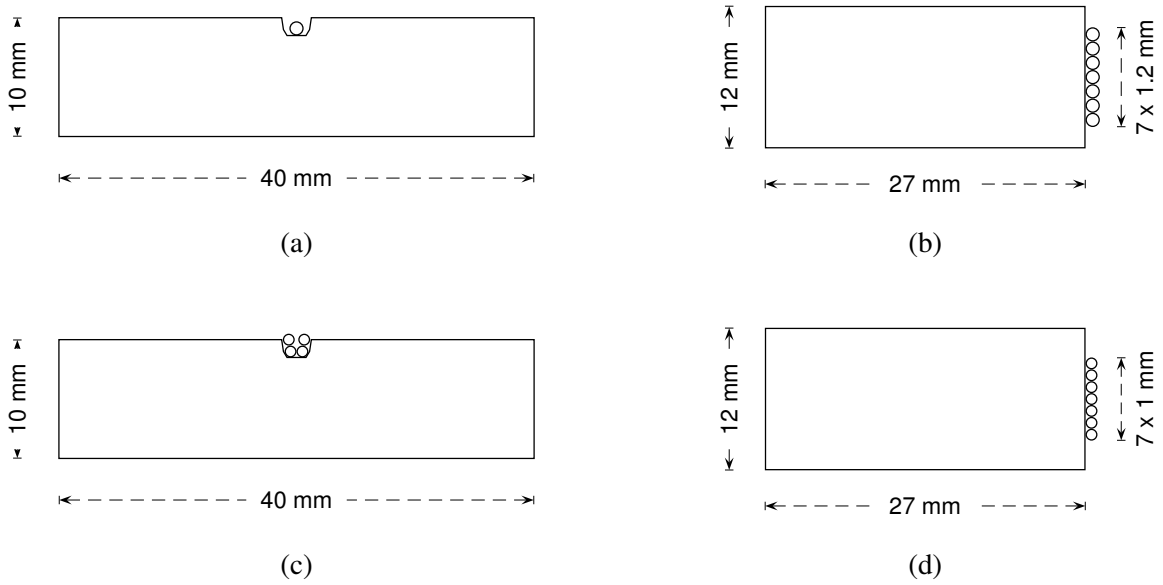

Figure 5: Tested configurations of the scintillator strip with WLS fibers:
(a) configuration *A*– MINOS strip with one Kuraray WLS fiber,
(b) configuration *B*– Bicron strip with 7 Kuraray WLS fibers,
(c) configuration *C*– MINOS strip with 4 Bicron WLS fibers,
(d) configuration *D*– Bicron strip with 7 Bicron WLS fibers.

tion [13], with one polystyrene double-clad fiber of 1.2 mm diameter with 175 ppm of Y-11 fluor produced by Kuraray Inc. Japan, inserted into the groove (Fig. 5(a)) [14]. The strip is then wrapped in black paper. The average light yield in configuration *A* was measured to be 10 photoelectrons on each side of the strip.

4.2 Configuration *B*

Configuration *B* consisted of a 1 m long clear Bicron© 404A fast scintillator strip with a 27×12 mm^2 profile [15], with 7 Kuraray Y-11 WLS fibers arranged along the narrow side (Fig. 5(b)). The fibers were attached to the strip in several points along the strip using reflective tape. The configuration was then wrapped with one layer of white Tyvek, and two layers of black paper.

The average light yield in the configuration *B* was measured to be 19 photoelectrons on each side.

4.3 Configuration *C*

Configuration *C* consisted of the MINOS strip [13], with 4 Bicron© BCF-92 WLS fibers of 1.0 mm diameter inserted into the groove (Fig. 5(c)) [16]. The average light yield in configuration *C* was measured to be 20 photoelectrons on each side.

4.4 Configuration D

Configuration D consisted of the Bicron© 404A strip [15], with 7 Bicron© BCF-92 WLS fibers of 1.0 mm diameter each arranged along the narrow side of the strip (Fig. 5(d)). The average light yield in configuration D was measured to be ~ 30 photoelectrons on each side.

The configurations C and D were selected for detailed position- and time-resolution studies.

5 Analysis

5.1 Analysis of the measurements performed with setup 1

5.1.1 Event selection

For setup 1 the off-line event selection was performed as follows:

1. Events in which the S4 signal is below the discriminator threshold, signalled by the end-of-scale value in the respective TDC channel, were rejected.
2. An amplitude threshold was imposed on the S4 counter signals to reject events with energies below the characteristic Landau distribution for the muon energy deposition.
3. Events in which the time of SiPM1 or SiPM2 shows the TDC end-of-scale value were rejected.
4. On rare occasions, the noise in the counter signals causes premature threshold crossing in the discriminator. Such events are characterized by a zero TDC readout in the respective channel, and were rejected. The fraction of such events was below 1% in all analyzed data samples.

5.1.2 Position resolution and the speed of signal propagation along the strip

In setup 1, the location of the muon impact was defined by the position x of the S4 counter along the axis of the tested strip. The center of the tested strip was assigned the relative position $x = 0$, and the x axis was oriented away from SiPM2 towards SiPM1. Five points along the strip were measured for the configurations C and D. The data for each point were collected over 7 to 12 hours in order to collect sufficient statistics (at least 500 events remaining per point after the selection cuts).

The observable with the best sensitivity to muon position along the strip is the time difference between the two SiPMs. Position is thus measured as,

$$x_{SiPM} = b_0 + v\frac{t_{SiPM_2} - t_{SiPM_1}}{2} = b_0 + v\frac{\Delta t}{2} \tag{2}$$

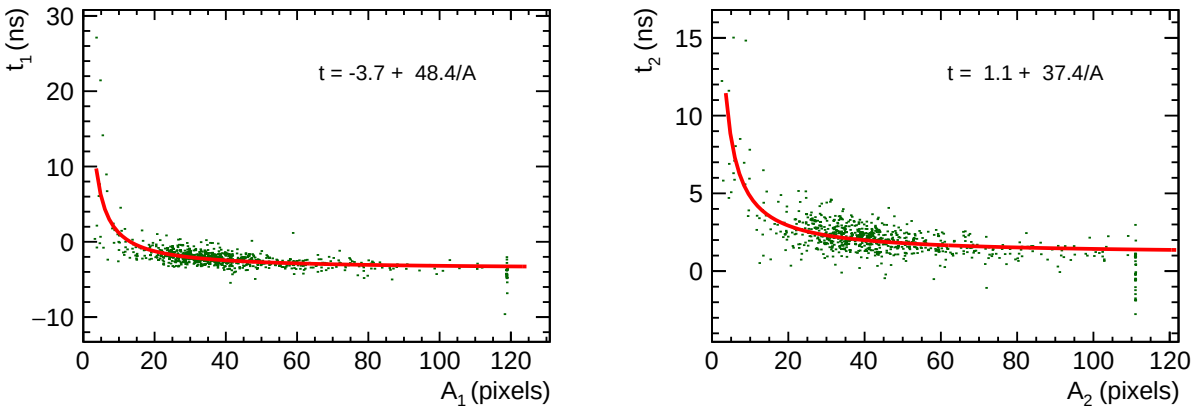

(a) (b)

Figure 6: Scatter plot of time vs. amplitude of SiPM1 (a) and SiPM2 (b), from the dataset taken at the S4 position $x = 0$ with configuration D, showing the amplitude-dependent delay of the timing signal from the discriminator. The function used for the correction of this effect is also shown (red line).

where b_0 is the offset and v is the speed of the signal propagation along the tested strip.

Timing of the signal rising edge using constant threshold discriminator has well-known amplitude-dependent variations. In the tested strips, the amplitude effect, beside worsening the time resolution also introduces a position-dependent bias because of the attenuation of light along the strip. The amplitude effect was corrected by fitting the function of the form $t = a_0 + a_1/A$, where A is the amplitude of the signal, to the scatter plot of time versus amplitude for each SiPM separately (Fig. 6). The uncertainty of the amplitude was neglected in the fit. The parameter a_1 obtained in the fit to the data collected at $x = 0$ (S4 at the center of the tested strip) was used to correct the amplitude effect at all measured positions for the same tested configuration.

The distribution of the variable $\Delta t/2$ after the amplitude correction is shown in Fig. 7 for the configuration D and $x = 0$. The standard deviation of the distribution, determined from a Gaussian fit, is the crucial parameter for the counter position resolution.

The speed of the signal propagation along the strip is determined from the linear fit to the scatter plot of x vs. $\Delta t/2$, as shown in Fig. 8. The uncertainty on $\Delta t/2$ was estimated from the scatter of the data, while the uncertainty on x was set to 1 cm, corresponding to the estimated precision of the position of the S4 counter.

The fitted value of the signal propagation speed along the strip in this example was 17.3 cm/ns. The average value of the standard deviation of $\Delta t/2$ from all 5 measured points was $\sigma_{\Delta t/2} = 0.45$ ns, which directly translates into the estimated position resolution $\sigma_x = 7.8$ cm for the configuration D. Beside the position resolution of the tested strip, this estimate contains contributions from the uncertainty of the muon impact position along the tested strip due to the width of S4 and the uncertainty due to the angular distribution of the muon tracks across the distance between S4 and

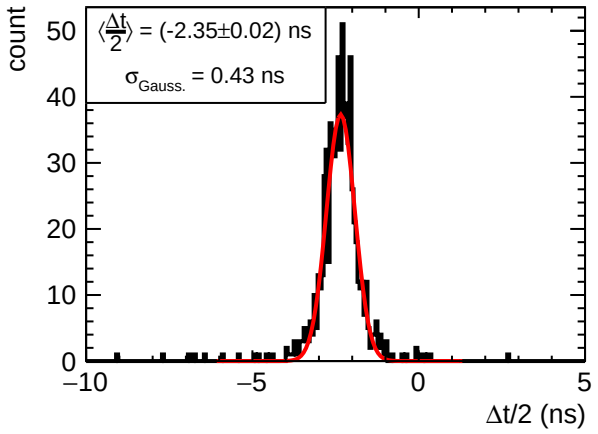

Figure 7: Distribution of the variable $\Delta t/2$ after the amplitude correction for the configuration D and $x = 0$.

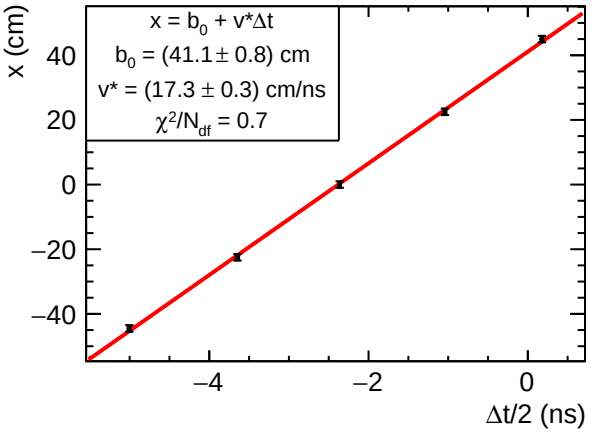

Figure 8: Scatter plot of x vs. $\frac{\Delta t}{2}$ for the configuration D.

the tested strip. This estimate of the coordinate resolution along the tested counter can thus be regarded as conservative.

5.1.3 Time resolution

The most direct way to measure strip time resolution is to analyze the distribution of differences between the mean time of the tested strip and the time of S4. As the mean time of the tested strip does not depend on the position of S4 along the tested strip, the data from all 5 studied S4 positions can be added up. The distribution of mean times is shown in Fig. 9(a) for the configuration D. The standard deviation of the fitted Gaussian curve is 0.52 ns. In this plot, the amplitude effect correction was applied to S4 in a similar way as to the SiPM.

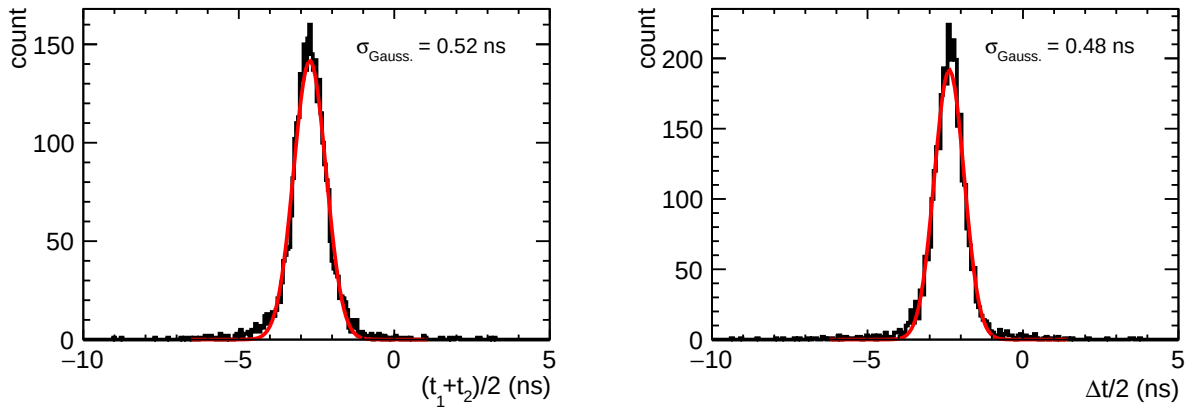

(a) (b)

Figure 9: Distribution of the mean times of the strip configuration D w.r.t. S4 in setup 1 (a) and distribution of the time difference between the two SiPM, plotted with correction for the muon position (b). Gaussian fit is shown as the red line in both plots.

The dominant contribution to the width of the distribution is the time resolution of the tested strip, but other contributions are also present, such as the time resolution of S4. Also, the width of the tested strip introduces a spread in the muon positions w.r.t. the PMT of S4. Another estimate of the time resolution of the tested strip can be inferred from the width of the distribution of $\Delta t/2 = (t_{\mathrm{SiPM1}} - t_{\mathrm{SiPM2}})/2$. A plot of $\Delta t/2 - x/v$ from all five datasets corresponding to different positions x of S4, is shown in Fig. 9(b) for the configuration D. The subtraction of the signal propagation delay x/v takes care of the dependence of $\Delta t/2$ on x. The standard deviation of the fitted Gaussian curve in this plot is 0.48 ns. The time resolution of S4 does not contribute to this width. Nevertheless, contributions from uncertainties other than the time resolution of the tested strip are still present, such as the uncertainties of x and v, and the muon-position spread due to the width of S4.

5.2 Analysis of measurements performed in setup 2

In setup 2 the position of the muon hit is determined from the time difference between S32 and S31, $\Delta t_{\mathrm{S3}} = t_{\mathrm{S32}} - t_{\mathrm{S31}}$ in the same way as for the tested strips (Eq. 2). The mean effective speed of the signal propagation along the scintillator strip, v_{sc}, is generally lower than the speed of light in the medium itself due to the light travelling under non-zero angle w.r.t. the strip and reflecting back into the medium multiple times before reaching the photo detector.

An example of the time distribution of the S32 channel is shown in Fig. 10. The distribution has a structured shape with a width of 9.7 ns, and a Gaussian smearing due to the time resolution of S31 and S32. The observed shape is mainly due to non-uniform detection efficiency of the system of counters. Calibration of the offset and the signal propagation speed is achieved by assigning the time at half maximum at the high-Δt edge of the distribution to the S31 end, and half-maximum at

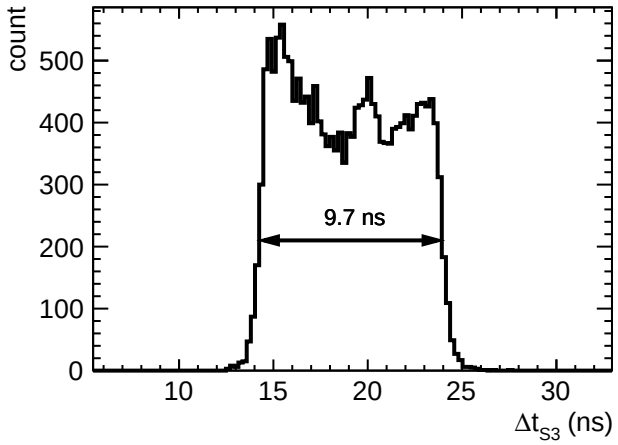

Figure 10: Time distribution of S32. The structure of the distribution reflects the variation of detection efficiency for cosmic muons along the setup.

the low-Δt edge to the S32 end. The length of the S3 scintillator in this test was $l = 60$ cm, leading to $v_{sc} = 12.4$ cm/ns.

5.2.1 Event selection

In setup 2 the off-line event selection was performed as follows:

1. An amplitude threshold was imposed on the sum of amplitudes of S31 and S32 to reject events at energies below the characteristic Landau distribution for the muon energy deposit.
2. Events in which the time of SiPM1, SiPM2 or S32 shows the TDC end-of-scale value were rejected.
3. Events with zero TDC reading in any of the channels were rejected. The fraction of such events was below 1% in all analyzed data sets.

5.2.2 Attenuation of light along strips with WLS fibers

Figure 11 shows a 2D plot of the SiPM1 amplitude vs. position along the S3 strip in the configuration *D*. Exponential fit to the data indicates an attenuation length for the light signal in this strip of $\lambda = 2.8$ m. The light intensity is well preserved by the WLS fibers along the strip, so muon position cannot be precisely determined from the signal attenuation.

5.2.3 Position resolution from Δt and the speed of signal propagation along the strip

The amplitude effect for setup 2 was corrected in a similar way as for setup 1. Figure 12 shows the scatter plot of time versus amplitude of both SiPMs from the dataset taken with the configuration

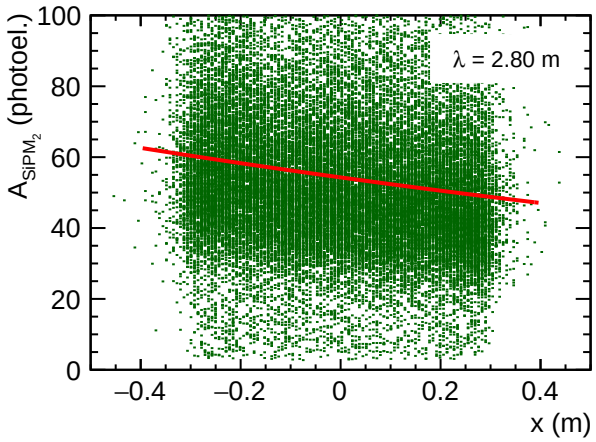

Figure 11: 2D plot of the SiPM2 amplitude vs. position event distribution along the S3 strip. Fit of the exponential function and the attenuation length are also shown.

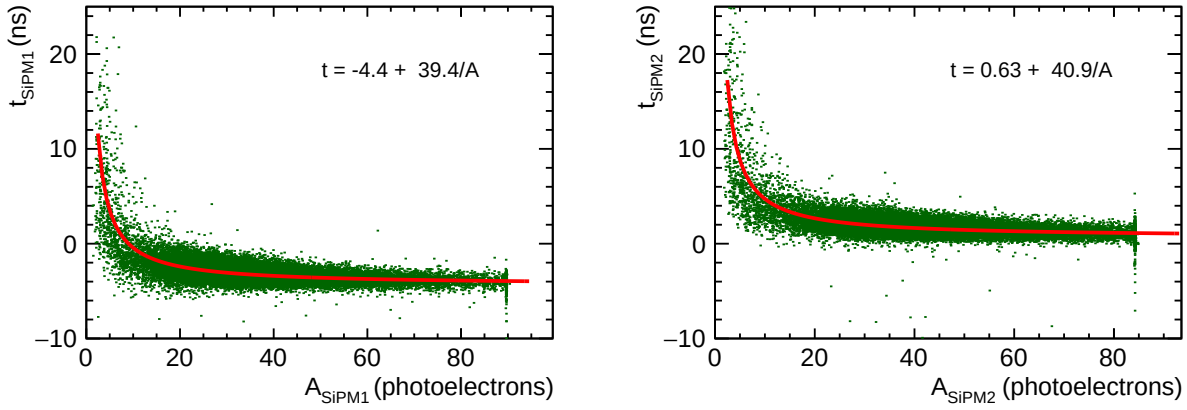

(a) (b)

Figure 12: Scatter plot of time vs. amplitude of SiPM1 (a) and SiPM2 (b), from the dataset taken with the configuration *D*, showing the amplitude-dependent delay of the timing signal from the discriminator. The function used for the correction of this efect (see legend) is also shown.

D. The fit of the function $t = a_0 + a_1/A$ is also shown. The uncertainty on the amplitude was neglected in the fit.

Figure 13(a) shows the scatter plot of the position x_{S3} measured with S3 vs. $(t_{\mathrm{SiPM}_2} - t_{\mathrm{SiPM}_1})/2$, after amplitude correction. Position x_{S3} is determined from t_{S32} assuming that the width at half maximum of the t_{S32} distribution (see Fig. 10) corresponds to the full length of the S3 strip.

The speed of the signal propagation along the strip determined from the linear fit to the scatter plot in this example is in excellent agreement with the result obtained with setup 1. The uncertainty

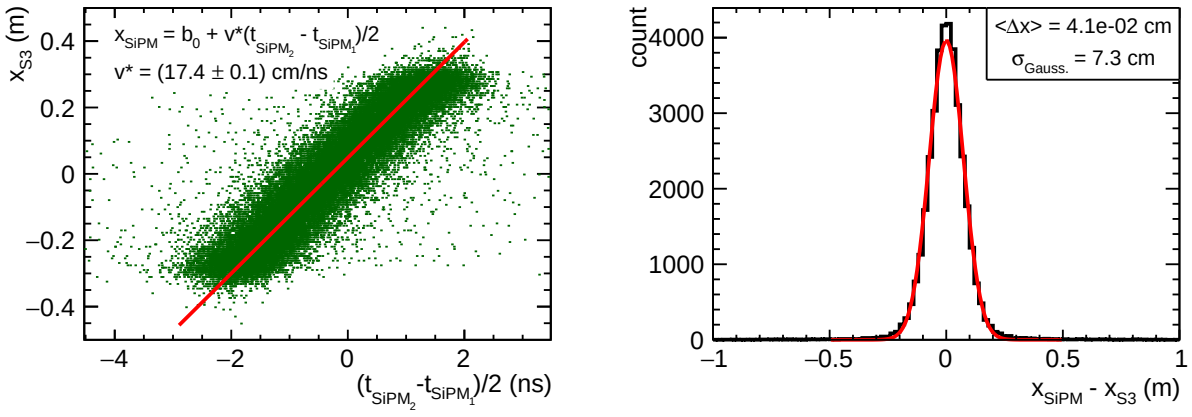

(a) (b)

Figure 13: (a) Scatter plot of the position along the strip measured with S3 vs. $(t_{\mathrm{SiPM}_2} - t_{\mathrm{SiPM}_1})/2$ in the Bicron© 404A configuration. Linear fit to the data is also shown. (b) Distribution of deviations of x_{SiPM} w.r.t x_{S3}.

of the position measurement is estimated from the distribution of the deviation of the position measured with SiPM w.r.t the position measured with S3 on the same dataset (Fig. 13(b)). The standard deviation estimated from the fitted Gaussian curve is $\sigma_{\mathrm{Gauss.}} = 7.3$ cm. This includes the position uncertainty of the tested strip, in addition to the position uncertainty of the reference strip, as well as the effect of the angular distribution of muons across the distance between the strip centers. It thus represents a conservative estimate of the position resolution of the tested strip.

5.2.4 Time resolution

The time resolution of the tested strip is directly measured by subtracting the average time of S31 and S32 from the average time of SiPM1 and SiPM2. The plot of the difference is shown in Fig. 14. The standard deviation of the distribution extracted from the Gaussian fit is 0.49 ns.

5.2.5 SiPM time resolution

For completeness, an estimate of the time resolution of the individual SiPM readouts is made as follows.

The S3 phototubes were used as the time reference for the respective SiPM signals. The time of S31 was subtracted from the time of SiPM1, and S32 was subtracted from SiPM2 as a first step of the analysis. Subsequently, the effect of the difference in the signal propagation speeds in S3 and the tested strip was corrected based on the position x measured by S3. The amplitude effect was corrected as described in Sec. 5.2.3.

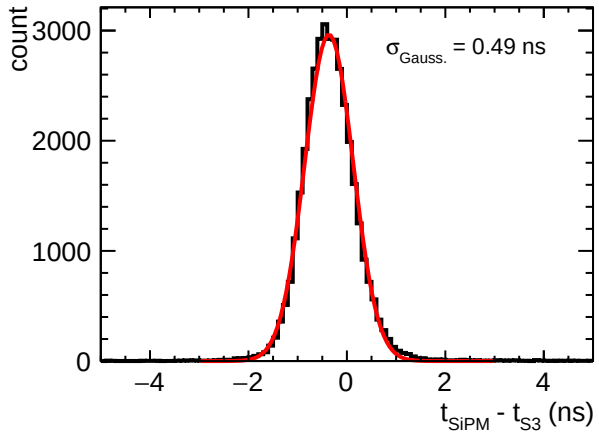

Figure 14: Distribution of the average-time differences between the tested strip and S3. Gaussian fit is also shown.

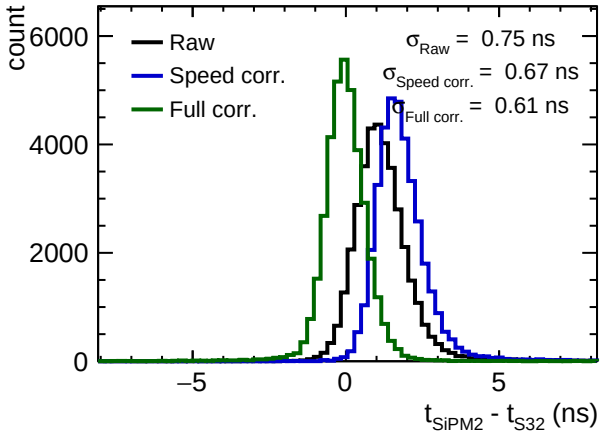

Figure 15: Time histogram for one of the SiPM channels w.r.t. the reference counter, without corrections (black), with correction for the difference in the signal propagation speed in the strips (blue) and with full correction including amplitude corrections for the tested strip and the reference strip (green).

The time resolution of the SiPM2 in the configuration *D* is shown in Fig. 15 for the raw case (without any corrections, black line), after correction for the difference in the signal propagation speed in the strips (blue line) and after the amplitude correction (green line). The numerical values shown in the figure represent fitted Gaussian standard deviations of the respective measured distributions (curves not shown).

Table 1: Measured performance of the individual SiPM readout channels for the configurations *C* and *D*.

Configuration	SiPM #	Light yield / muon (photoelectrons)	$\sigma_{t,SiPM}$ (ns)
C	1	21	1.12
	2	20	1.17
D	1	31	0.67
	2	36	0.61

Table 2: Measured properties of the strip configurations *C* and *D*.

Configuration	σ_x (setup 1) (cm)	σ_x (setup 2) (cm)	$\sigma_{t,strip}$ (ns)	Speed of light (cm/ns)
C	14.8	14.8	0.91	18.1
D	7.8	7.3	0.48	17.2

6 Results

Table 1 summarizes the measured performance of the individual SiPM readout channels for the configurations *C* and *D*.

Table 2 summarizes the results regarding the strip configurations as a whole. The difference in the resolutions for the two configurations is larger than the ratio of the statistical factors corresponding to the photon yield per muon in each configuration. This indicates that other factors influence the time and the position resolutions besides the statistical effect of the photon yield. These additional effects include the properties of the scintillator and the WLS fiber materials such as the light emission time, the geometry of the configuration, the location of the WLS fibers etc.

The best directly measured position resolution is 7.3 cm, and has been achieved with the configuration *D*.

7 Conclusions

Prototype scintilator+WLS strip configurations with SiPM readout for the muon system for future colliders were tested for light yield, position resolution and time resolution. Depending on the configuration, a light yield in single SiPM of up to 36 photoelectrons per muon has been achieved. Two different setups were used for position- and time-resolution measurements. In one setup, the muon impact position was determined by coincidence requirement with a small-area counter. In the other, a reference strip with vacuum PMT parallel to the tested strip was used to measure position independently.

Strip time resolution of 0.5 ns and position resolution of ~ 7 cm were achieved. Tests with more

precise timing and/or position reference, such as in the test-beam, will yield results with higher precision.

References

[1] URL: https://www.linearcollider.org/.

[2] URL: http://tlep.web.cern.ch/.

[3] URL: http://cepc.ihep.ac.cn/.

[4] H. Aihara, P. Burrows, M. Oreglia, eds., *SiD Letter of Intent*, SLAC-R-989 – FERMILAB-LOI-2009-01 – FERMILAB-PUB-09-681-E, arXiv:0911.0006, 2009.

[5] ILD Concept Group, *The International Large Detector – Letter of Intent*, Report DESY 2009/87 – Fermilab PUB-09-682-E – KEK Report 2009-6, http://ilcild.org/, 2010.

[6] J. Repond, *Recent DHCAL Developments*, International Workshop on Future Linear Colliders (LCWS13) Tokyo, Japan, 11-15 November 2013, arXiv:1312.3868.

[7] T. Behnke et al., eds., *The International Linear Collider - Technical Design Report*, vol. 4: Detectors, ILC-REPORT-2013-040, arXiv:1306.6329, International Linear Collider, 2013, URL: http://www.linearcollider.org/ILC/TDR.

[8] K. Woodruf et al., *Studies of the Cosmic Ray Flux in MicroBooNE*, APS April Meeting April 5–8, 2014, Savannah, Georgia, URL: http://www-microboone.fnal.gov/talks/APSApril_woodruff.pdf.

[9] URL: https://www.hamamatsu.com/sp/hpe/HamamatsuNews/HamamatsuNews_0109.pdf.

[10] URL: http://vinhep.vin.bg.ac.rs/strahinja-software/SiPM/WienerDAQdocu.pdf.

[11] B. Dolgoshein et al., *Status report on silicon photomultiplier development and its applications*, Nucl. Inst. Meth. **A 563** 2 (2006) 368, URL: http://www.sciencedirect.com/science/article/pii/S0168900206004578.

[12] Valery Evdokimov, *Light collection from scintillation counters using WLS fibers and bars*, AIP Conf. Proc. **450** (1998) 300, DOI: 10.1063/1.56976.

[13] The MINOS Collaboration, *The magnetized steel and scintillator calorimeters of the MINOS experiment*, Nucl. Inst. Meth. **A 596** (2008) 190, DOI: 10.1016/j.nima.2008.08.003.

[14] URL: http://kuraraypsf.jp/psf/ws.html.

[15] URL: http://www.crystals.saint-gobain.com/uploadedFiles/SG-Crystals/Documents/SGC%20BC400-404-408-412-416%20Data%20Sheet.pdf.

[16] URL: http://www.crystals.saint-gobain.com/uploadedFiles/SG-Crystals/Documents/SGC%20Fibers%20Brochure.pdf.